Comparison of methods for online inspection of apple internal quality

M. van Dael[1], P. Verboven[1], L. Van Hoorebeke[2], J. Sijbers[3], B. Nicolai[1]

[1] Flanders Centre of Postharvest Technology / BIOSYST-MeBioS, University of Leuven, Willem de Croylaan 42, 3001 Leuven, Belgium

[2] UGCT, Dept. Physics and Astronomy, Ghent University, Proeftuinstraat 86, 9000 Ghent, Belgium

[3] iMinds-Vision Lab, Department of Physics, University of Antwerp, Universiteitsplein 1, B-2610 Wilrijk, Belgium

Abstract
Various methods for online quality inspection using X-ray (CT) are available. Here, two novel methods are compared. The first approach uses 3D vision in combination with deformable shape models to normalize X-ray radiographs for the sample shape, revealing internal properties and/or defects. The second approach reconstructs the sample based on limited data obtained by combining the translational movement of the sample on the conveyor belt with a limited sample rotation. Both methods have advantages and disadvantages and a choice between them should be motivated by application-specific requirements.

Keywords: X-ray, inspection, online, agrofood

1. Materials and Methods

1.1. Dataset

26 apple fruits of the Braeburn cultivar were harvested in November 2014 and stored at defect inducing gas conditions (1°C / 2.5 % O_2 / > 5 % CO_2). The apples were stacked in a crate containing a matrix of polystyrene sheets, positioned in a way so these would not limit the airflow. At the start of the experiment and every 6 to 8 weeks during storage the sample crate was imaged using a Siemens SOMATOM Definition Flash CT scanner at the Gasthuisberg University Hospital in Leuven, resulting in 5 timepoints. Axial slices through 2 samples are shown in Figure 1 for all 5 timepoints, showing the developing defect as a locally decreasing density mainly due to water displacement inside the fruit.

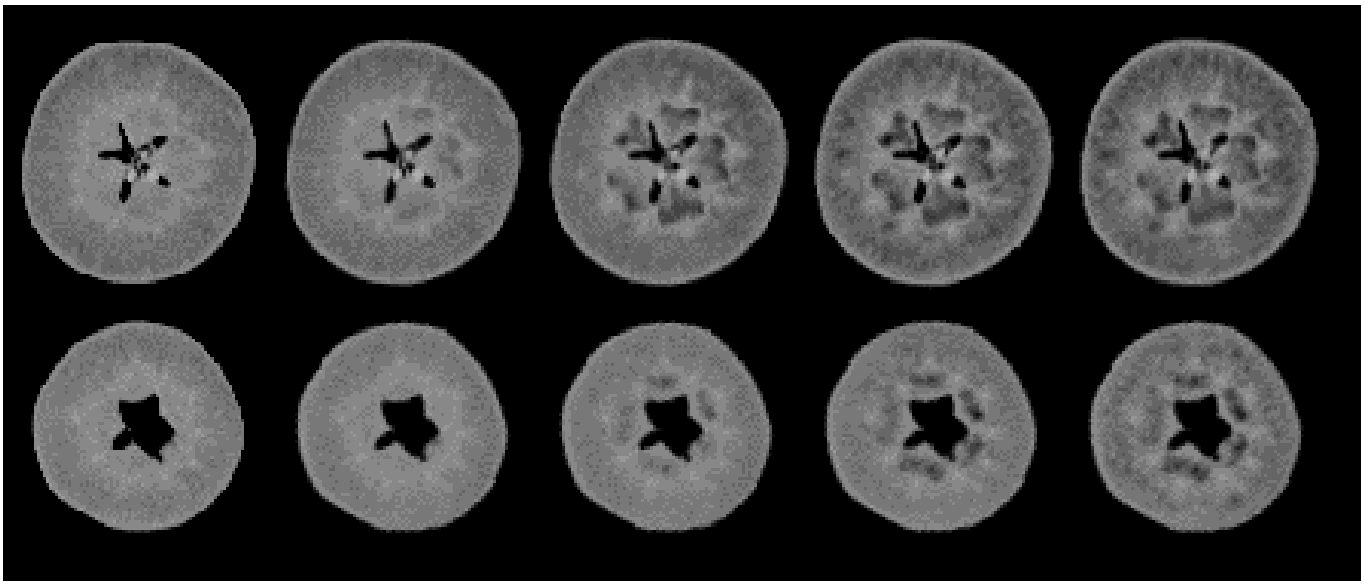

Figure 1. Overview of CT image slices of 2 Braeburn apples. The different columns correspond to different time points in storage (26/11/2014, 19/01/2015, 02/03/2015, 20/04/2015, 29/06/2014).

All resulting scans were rigidly registered to the first time point and subtracted from it to determine internal changes occurring in the samples during storage. These differential images could be used to accurately visualize change during the storage period, as shown in Figure 2. The tissue close to the core in between the main vascular bundles is first affected. As time progresses the affected tissue volume increases in all directions.

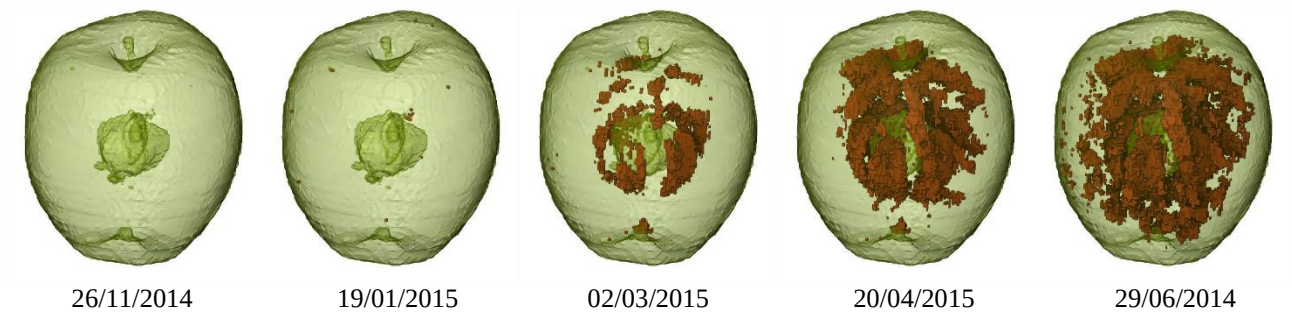

Figure 2. 3D-rendering of the segmented defect (colored in red) in the total apple volume as a function of storage time. The example is given for a Braeburn apple from Italian origin.

1.2. Multisensor inspection

A 3D vision system and radiograph linescanner are installed on a conveyor belt. A statistical shape model [1] is fitted to the pointcloud generated by the 3D vision system using a decoupled iterative closest point alignment [2] and least squares fit. This reference shape is voxelized using a spherically resampled density distribution and a radiograph is simulated using the ASTRA toolbox [3], [4]. This simulated radiograph is subtracted from the measured radiograph, resulting in a residual image which can be used to asses the possible presence of defects or not expected properties inside the sample. A flowchart of this method is shown in Figure 3.

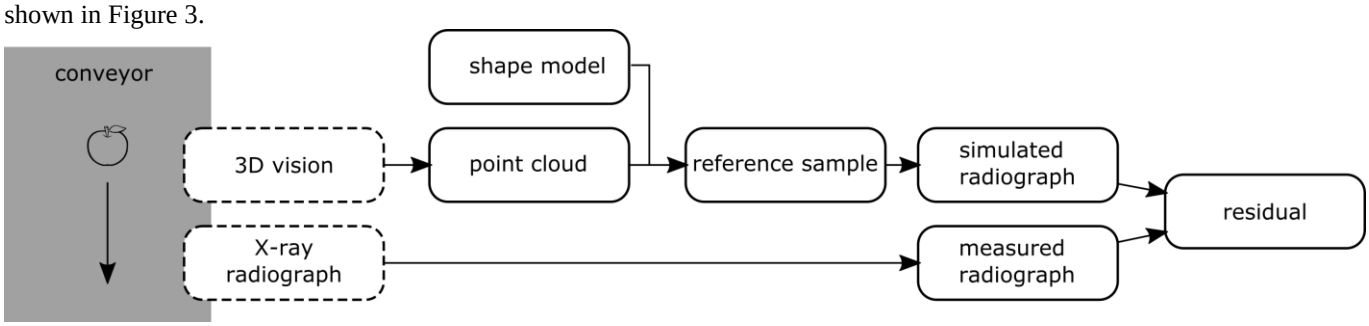

Figure 3: Flowchart of the multisensor inspection method

1.3. Reconstruction from limited data

The translational movement of a sample on a conveyor belt passing between an X-ray source and detector, combined with a limited rotation of the sample (see Figure 4) as described in [5] is used to obtain projections from a sufficient angular range to allow for SIRT-based reconstruction. Classic, defect-specific image processing methods are then used to grade the inspected samples based on these reconstructions.

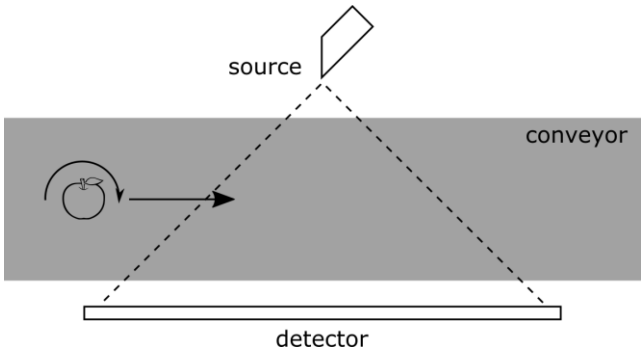

Figure 4: Obtaining projections by using the translation between source and detector and a small rotation of the sample.

2. Results and discussion

2.1. Multisensor inspection

Figure 5 shows the complete model used to construct the reference samples. Figure 5(a) shows the first two components of the statistical shape model describing the sample surface with weights of -3, 0 and 3 standard deviations. Notice how the first

component mainly describes samples size, while the second component starts deforming the shape non-uniformly. Figure 5(b) shows the sphericaly resampled density distribution used to construct the reference sample. From left to right, the position changes from the sample center tot he sample surface. From top to bottom, the vertical angle with relation to the sample center (elevation) increases. The density distribution is averaged over the horizontal angle with relation to the center (azimuth), since it is very difficult to estimate the orientation of the sample core along this axis purely from information from the outer shape.

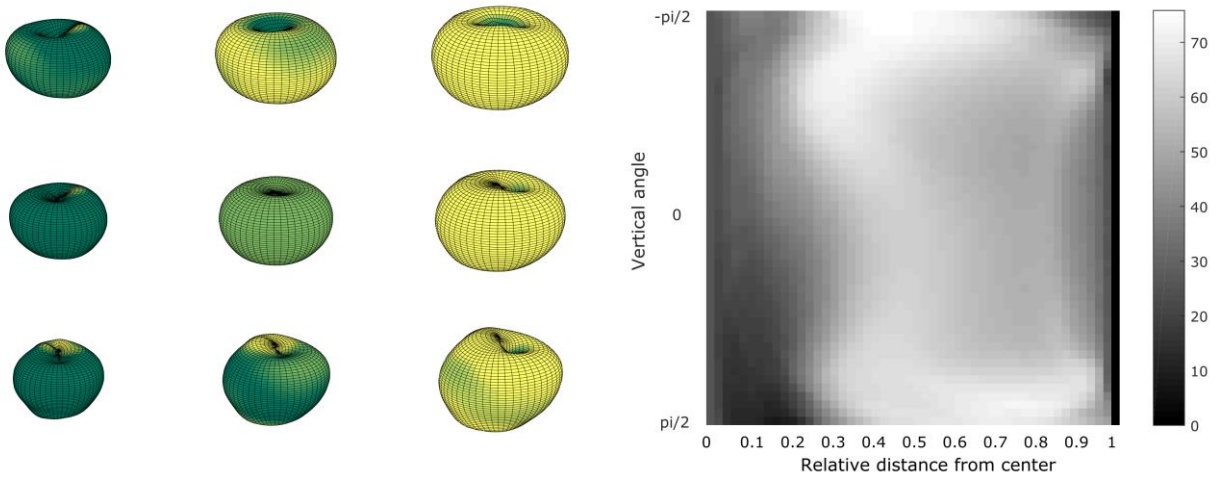

(a) (b)

Figure 5: Image (a) shows the first two components of the statistical shape model with weights of -3, 0 and 3 standard deviations. Image (b) shows the sphericaly resampled density distribution used to construct the reference sample.

Figure 6(a) shows sagittal slices through 7 samples at the start of the experiment, i.e. without already developed defects. Row (b) shows the statistical shape model as it was fitted to the surface point clouds of the respective samples. Row (c) shows sagittal slices through the respective samples, created by revoxelizing the fitted shape model using the density distribution shown in Figure (b). Note that the apple cores display a very irregular 3-dimensional shape in row (a). Using the averaged density distribution to voxelize the model, however, results in an approximation of its location and size as shown in row (c). Other patterns such as, for example, higer density near the main vascular bundles around the core of the fruit, are adequately reproduced.

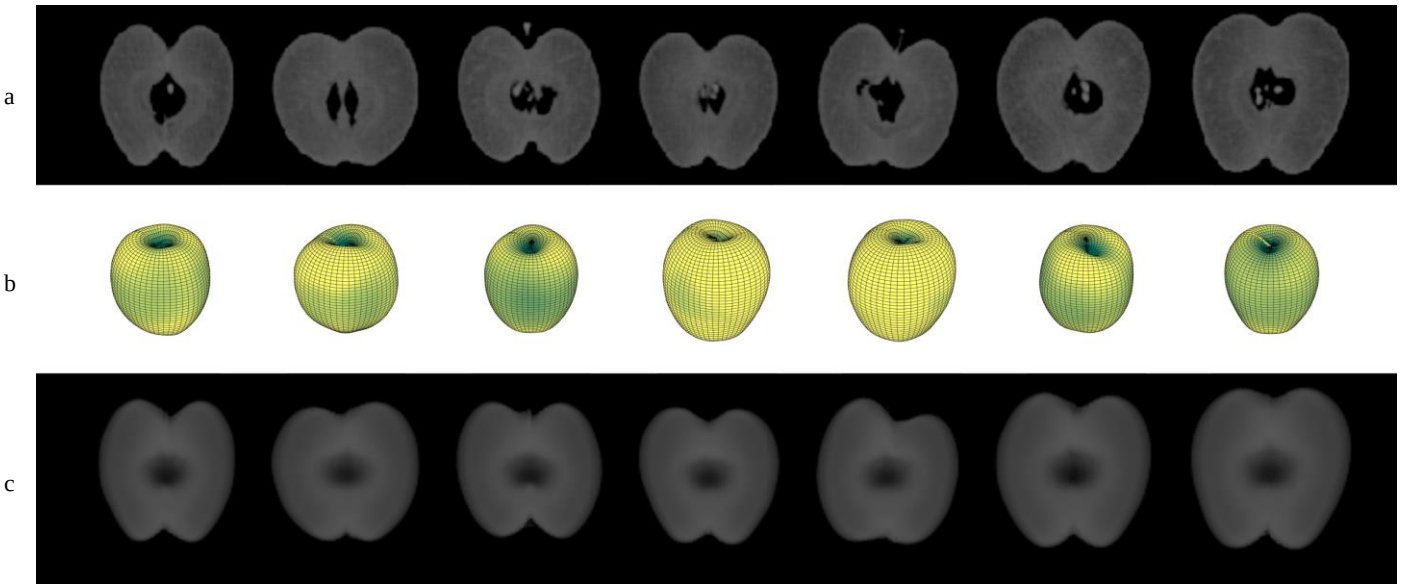

Figure 6: Row (a) shows sagittal slices trough CT scans of 7 samples at the first timepoint. Row (b) shows the shape model fitted to the sample surface. Row (c) shows sagittal slices through the respective samples, creating by revoxelizing the fitted shape model using the density distribution shown in Figure (b)

Figure 7 shows the outputs of the multisensor inspection method. Row (a) shows radiographs of 5 samples with defects, while row (b) shows identical radiographs but simulated form their respective reference samples with the same fruit shape. Note that

for both these rows image contrast has been increased for visualization purposes. Row (c) shows the difference or residual images between rows (a) and (b), with red colors indicating positive values and blue colors indicating negative values. The shape of the samples is accurately described, and in general the estimation of the internal density distribution seems acceptable. Some patterns still arise though. Firstly, the core lights up in the residual images, characterized by an alternation of positive values between and negative values inside the seed lobes on the residual images. This can be contributed to the averaging of the density distribution along the horizontal axis (azimuth) and was expected. Secondly, all residual images show positive values along the sample edge. This effect was unexpected and is subject to future improvements in the sampling and resampling procedure.

a

b

c

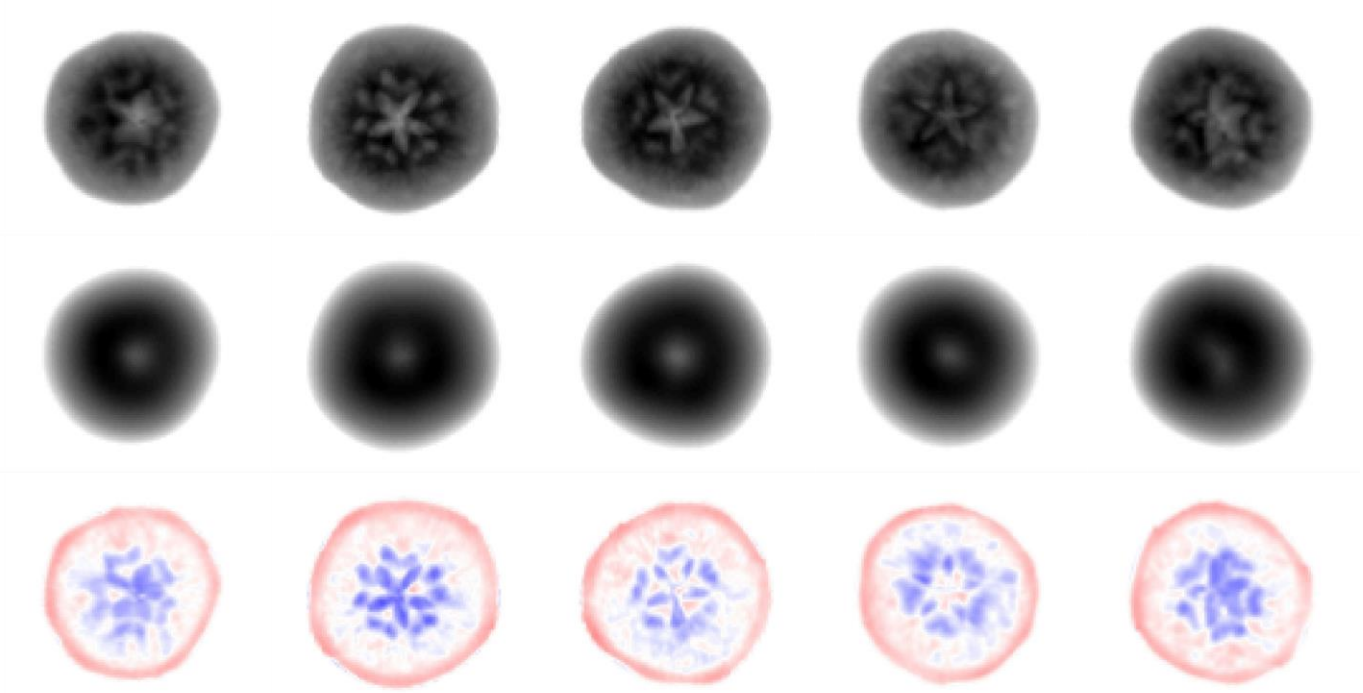

Figure 7: Row (a) shows radiographs from samples with defects. Row (b) shows simulated projections from the corresponding reference samples. Contrast in rows (a) and (b) has been increased for visualization purposes. Row (c) shows the residual images generated by subtracting the projections in rows (a) and (b).

Figure 8 shows the total sum of pixel values (scaled between -1 and 1) on the y-axis versus the total sum of absolute voxel values of the difference volumes (scaled between -255 and 255) as described in section 1.1 (x-axis), which can be regarded as a reference directly from CT scans. The different colors indicate the scans performed at the different time points during storage. Although only basic assumptions regarding the samples' internal density distribution were made, the multisensor inspection method can quite accurately ($R^2 = 0.80$) predict the degree of defects based on a single radiograph in combination with the shape model.

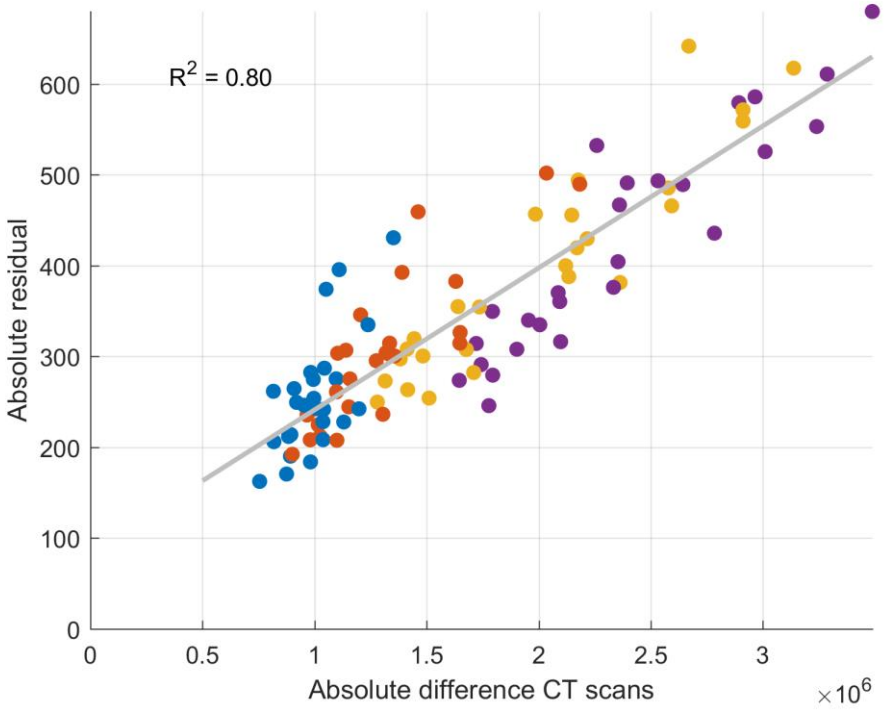

Figure 8: Summed absolute values of the residual images (Figure 7, c) against the sum absolute voxel values (scaled between -255 and 255) in the CT scans relative to the reference scan.

2.2. Reconstruction from limited data

To evaluate the performance of a CT inspection mehod using limited projection data, first a threshold to segment defects from the reconstructions was validated on a standard CT-scan. Results are shown if Figure 9, plotting the segmented volumes in mm^3 (y-axis) using three different threshold levels versus the total sum of absolute voxel values of the difference volumes as described in section 1.1 (x-axis). The threshold resulting in maximal correlation was 42 on an 8-bit grayscale, with an R^2 value of 0.82 .

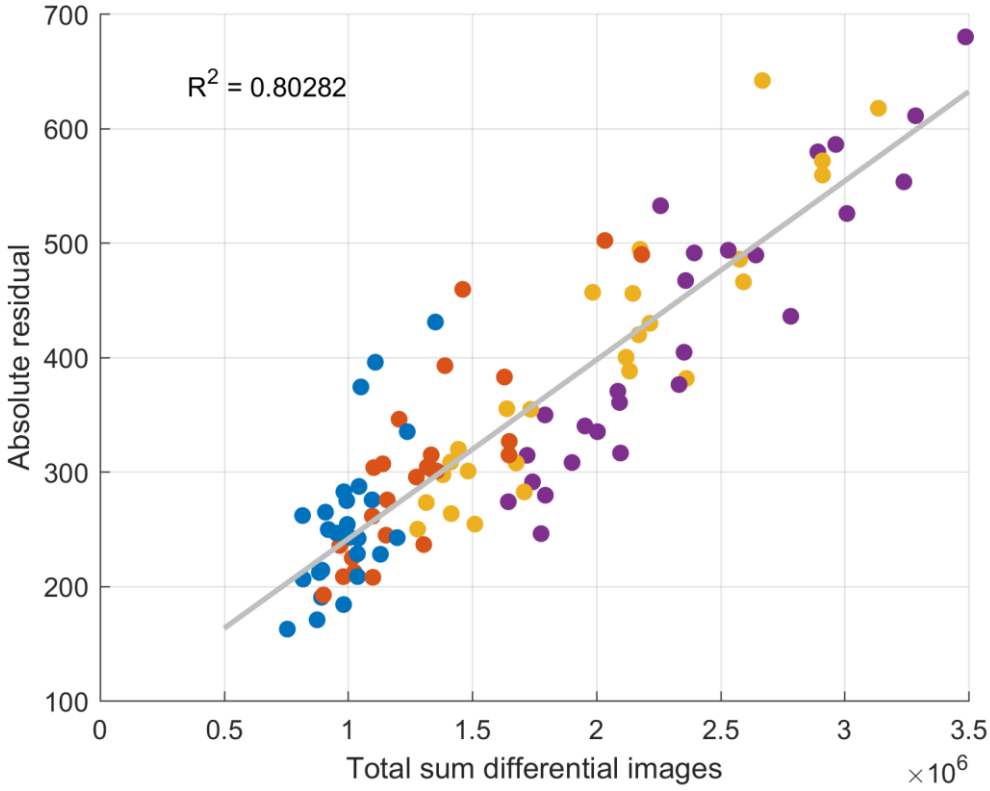

Figure 9: Correlation between total sum of voxel values in the differential images (x-axis) versus defect volumes segmented using a simple threshold of the CT scan (y-axis). Different colors indicate threshold levels of 38, 41 and 44 on an 8-bit grayscale.

Figure 10 shows the defect volumes segmented from the reconstructions from limited data using the threshold level previously determined. These results show that the correlation clearly increases with the number of projections used for the reconstructions with R^2 values of 0.68, 0.81 and 0.83 for defect volume segmentations from reconstructions with 5, 10 and 20 projections respectively. Notice how the total segmented volume also decreases with an increased number of projections approximating the segmented volumes form complete scans as shown in Figure 9 with increasing number of projections.

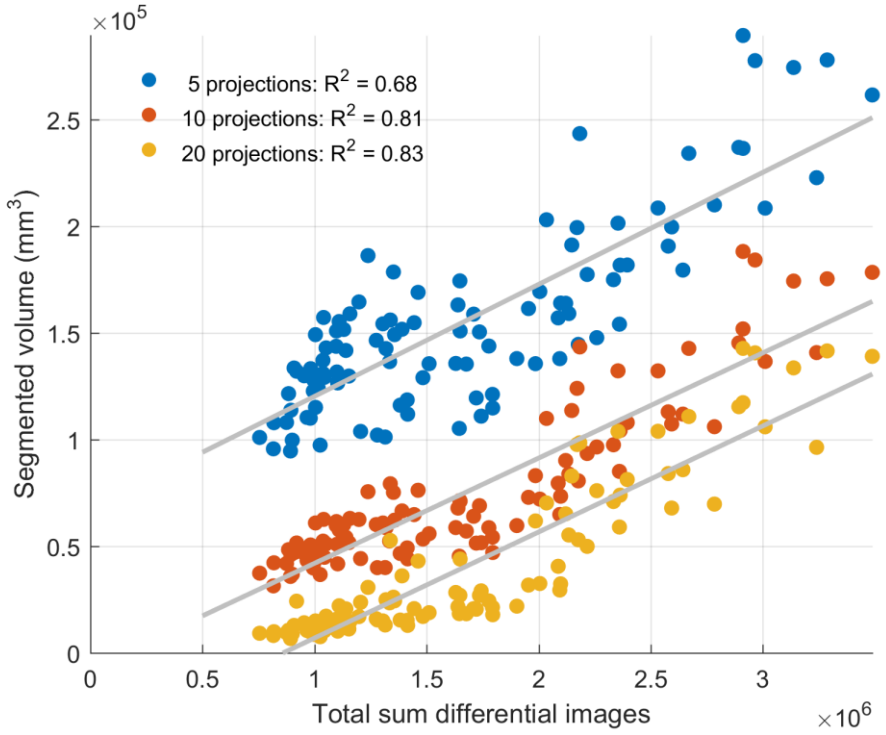

Figure 10. Correlation between total sum of voxel values in the differential images (x-axis) versus defect volumes segmented using a simple threshold (41 on an 8-bit grayscale) of a CT scan (y-axis). Different colors indicate reconstructions from 5, 10 and 20 projections.

3. Discussion and conclusion

Two methods based on X-ray imaging were compared for detecting defects in fruit. Both methods can detect the disorder but some differences are worth noting. The multisensor approach detects the presence of a defect or disorder quite accurately (R^2 = 0.80) including a estimate of the relative size of the defect but it is not suited for more advanced shape analysis as only a 2D image is recorded. It is fast and cheap though, and since it detects deviations from an ideal reference, it is more flexible with regard to the types of defects it can detect. The limited reconstruction-based method is more expensive as a projection need to be recorded from different angles. It requires a large area X-ray detector and appropriate hardware to rotate samples in a controlled way. At least 10 projections are needed to accurately quantify the disorder (R^2 = 0.81). However, the reconstruction allows for a more detailed analysis and quantification of internal properties. Image processing methods have to be developed for every type of defect, however, making it less flexible. Based on these results it can be concluded that both methods have advantages and disadvantages and a selection should be based on a detailed analysis of application-specific requirements.

Acknowledgements

We would like to thank the Flanders Fund for Scientific Research (FWO, SBO 120033), the Monalisa project of the Research Centre for Agriculture and Forestry Laimburg (Italy), the Hercules foundation (project AKUL 09/001), and the EC (project PicknPack FP7-311987) for financial support. The opinions expressed in this document do by no means reflect their official opinion or that of its representatives.

References

[1] F. Danckaers, T. Huysmans, M. van Dael, P. Verboven, B. Nicolai, and J. Sijbers, "Building a statistical shape model of the apple from corresponded surfaces.," *Chem. Eng. Trans.*, vol. 44, pp. 49–54, 2015.

[2] P. J. Besl and H. D. McKay, "A method for registration of 3-D shapes," *IEEE Trans. Pattern Anal. Mach. Intell.*, vol. 14, no. 2, pp. 239–256, 1992.

[3] W. van Aarle, W. J. Palenstijn, J. De Beenhouwer, T. Altantzis, S. Bals, K. J. Batenburg, and J. Sijbers, "The ASTRA Toolbox: A platform for advanced algorithm development in electron tomography," *Ultramicroscopy*, vol. 157, pp. 35–47, 2015.

[4] W. J. Palenstijn, K. J. Batenburg, and J. Sijbers, "Performance improvements for iterative electron tomography reconstruction using graphics processing units (GPUs).," *J. Struct. Biol.*, vol. 176, no. 2, pp. 250–3, Nov. 2011.

[5] T. De Schryver, J. Dhaene, M. Dierick, M. N. Boone, E. Janssens, J. Sijbers, M. van Dael, P. Verboven, B. Nicolai, and L. Van Hoorebeke, "In-line NDT with X-Ray CT combining sample rotation and translation," *NDT E Int.*, vol. 84, pp. 89–98, 2016.